Current Biology 22, 1891–1899, October 23, 2012 ©2012 Elsevier Ltd All rights reserved http://dx.doi.org/10.1016/j.cub.2012.08.024

Article

A Genome-wide Functional Screen Shows MAGI-1 Is an L1CAM-Dependent Stabilizer of Apical Junctions in *C. elegans*

Allison M. Lynch,[1,2] Theresa Grana,[3] Elisabeth Cox-Paulson,[4] Annabelle Couthier,[5] Michel Cameron,[6] Ian Chin-Sang,[6] Jonathan Pettitt,[5] and Jeff Hardin[1,2,*]

[1]Graduate Program in Genetics
[2]Department of Zoology
University of Wisconsin-Madison, 1117 W. Johnson Street, Madison, WI 53706, USA
[3]Department of Biological Sciences, University of Mary Washington, 1301 College Ave., Fredericksburg, VA 22401, USA
[4]Department of Biology, State University of New York at Geneseo, 353 Integrated Science Center, 1 College Circle, Geneseo, NY 14454, USA
[5]Department of Molecular and Cell Biology, University of Aberdeen Institute of Medical Sciences, Aberdeen AB25 2ZD, UK
[6]Department of Biology, Queen's University, Kingston, Ontario K7L 3N6, Canada

Summary

Background: In multicellular organisms, cell-cell junctions are involved in many aspects of tissue morphogenesis. α-catenin links the cadherin-catenin complex (CCC) to the actin cytoskeleton, stabilizing cadherin-dependent adhesions.
Results: To identify modulators of cadherin-based cell adhesion, we conducted a genome-wide RNAi screen in *C. elegans* and uncovered MAGI-1, a highly conserved protein scaffold. Loss of *magi-1* function in wild-type embryos results in disorganized epithelial migration and occasional morphogenetic failure. MAGI-1 physically interacts with the putative actin regulator AFD-1/afadin; knocking down *magi-1* or *afd-1* function in a hypomorphic α-catenin background leads to complete morphogenetic failure and actin disorganization in the embryonic epidermis. MAGI-1 and AFD-1 localize to a unique domain in the apical junction and normal accumulation of MAGI-1 at junctions requires SAX-7/L1CAM, which can bind MAGI-1 via its C terminus. Depletion of MAGI-1 leads to loss of spatial segregation and expansion of apical junctional domains and greater mobility of junctional proteins.
Conclusions: Our screen is the first genome-wide approach to identify proteins that function synergistically with the CCC during epidermal morphogenesis in a living embryo. We demonstrate novel physical interactions between MAGI-1, AFD-1/afadin, and SAX-7/L1CAM, which are part of a functional interactome that includes components of the core CCC. Our results further suggest that MAGI-1 helps to partition and maintain a stable, spatially ordered apical junction during morphogenesis.

Introduction

Adhesion between epithelial cells is essential for the dramatic changes in cell shape, cell-cell contacts, and cellular rearrangements that occur during morphogenesis [1]. *Caenorhabditis elegans* provide a powerful genetic model in which to study modulation of cell-cell junctions during development due to the simplicity of the *C. elegans* apical junction (CeAJ). The CeAJ contains three domains [2]: an apical membrane domain, a classical cadherin-catenin complex (CCC) [3], and a more basal DLG-1/AJM-1 complex [4, 5]. Although important for morphogenesis, the *C. elegans* CCC is not essential for general cell-cell adhesion in embryos [3], unlike other systems [6–8], suggesting that other proteins act redundantly with the CCC during development.

We used a genome-wide RNAi screen to identify proteins that exhibit functional redundancy or synergy with the CCC during embryonic development and uncovered MAGI-1, an inverted MAGUK (Membrane Associated GUanylate Kinase) family protein. MAGUKs can assemble multiprotein complexes at sites of cell-cell adhesion, and are key organizers of cell-cell junctions [9]. The *C. elegans magi-1* locus encodes a short isoform, MAGI-1S, containing two WW and five PDZ domains, and a long isoform, MAGI-1L, which has an additional N-terminal GUK domain [10]. Reduction of MAGI-1L results in defective mechanosensory memory acquisition and olfactory and gustatory associative learning [10, 11]. Furthermore, memory consolidation and nose-touch response depend on the ability of MAGI-1 to interact with β-catenin at synapses [11].

Here we show that MAGI-1 physically interacts with AFD-1/afadin, which itself synergizes with the CCC during morphogenesis. In contrast to a previous report [12], we use immunolocalization of endogenous proteins to show that MAGI-1 localizes between the CCC and DLG-1/AJM-1 complex and that localization is partially dependent on the MAGI-1 binding partner SAX-7/L1CAM. Finally, we show that MAGI-1 acts to maintain the spatial segregation of apical junctional complexes during embryonic morphogenesis. Our screen is the first genome-wide approach to identifying proteins that function synergistically with the CCC in a living organism and identifies in vivo roles for a MAGI protein during epithelial morphogenesis.

Results

A Genome-wide RNAi Screen Identifies Genetic Interactors with the CCC

To identify functional interactors with the *C. elegans* CCC, we screened an RNAi bacterial expression library that targets ~86% of *C. elegans* open reading frames [13] in worms homozygous for a hypomorphic allele of α-catenin, *hmp-1(fe4)*. *hmp-1(fe4)* homozygotes exhibit ~70% lethality and defects in actin organization and body morphology [14]. Induced bacteria from the library were fed to *hmp-1(fe4)* worms and clones that increased lethality in *hmp-1(fe4)* worms were identified (Figure 1A). Clones that had not been previously reported to cause lethality were rescreened in *hmp-1(fe4)* and wild-type (WT) worms; we eliminated clones that caused significant lethality in WT worms in our hands, even though they had not been previously reported to do so. The remaining clones were screened a final time in *hmp-1(fe4)* and WT worms to

*Correspondence: jdhardin@wisc.edu

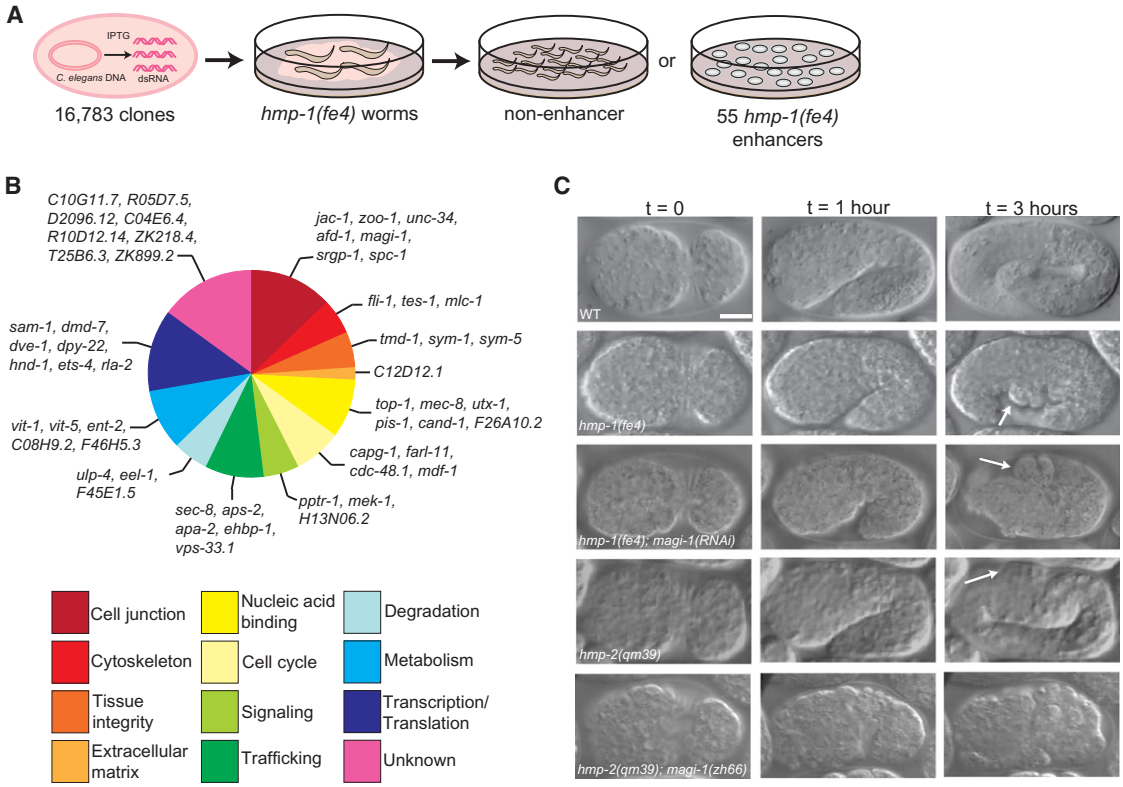

Figure 1. An Enhancer Screen Identifies Putative Adhesion Modulators during *C. elegans* Morphogenesis

(A) We screened a library of 16,783 RNAi feeding clones to identify enhancers of a hypomorphic allele of α-catenin, *hmp-1(fe4)*. Each bacterial clone was fed to WT, and *hmp-1(fe4)* worms and phenotypes were assessed in the next generation. Enhancers increased lethality in *hmp-1(fe4)* embryos to >83% while causing <10% lethality in WT embryos.

(B) Putative functions for enhancers were determined using literature searches, BLAST, and ClustalW comparisons of protein sequence, identification of domains using Pfam, and NCBI KOG description. Functional groups were based on previously published categories [37, 38].

(C) Knocking down *magi-1* enhances the penetrance and severity of *hmp-1(fe4)* and *hmp-2(qm39)* phenotypes. WT embryos enclose (t = 0), turn (t = 1 hr), and elongate ~4-fold their original length before hatching (t = 3 hr). *hmp-1(fe4)* embryos enclose (t = 0) but fail to fully elongate, developing body shape defects (arrow, t = 3 hr). The majority of *hmp-1(fe4); magi-1(RNAi)* embryos enclose (t = 0) but almost immediately retract dorsally and arrest, with a characteristic humpback phenotype (arrow, t = 3 hr). *hmp-2(qm39)* embryos enclose (t = 0) and elongate, occasionally developing mild body shape defects (arrow, t = 3 hr). A significant fraction of *hmp-2(qm39); magi-1(zh66)* embryos fail to enclose and rupture (t = 3 hr). Scale bar represents 10 μm.

count the percentage of dead embryos. Our screen identified 55 genes that when knocked down by feeding RNAi enhanced the *hmp-1(fe4)* phenotype to >83% lethality but did not produce severe phenotypes in WT worms (Figure 1B; see also Table S1 available online).

Knocking Down *magi-1* Enhances the Penetrance and Severity of *hmp-1(fe4)* Phenotypes

Our screen identified several putative junctional proteins including *magi-1*. *magi-1(RNAi)* enhances the lethality of *hmp-1(fe4)* embryos to 99% (n = 399) (Figure 1C; Movie S1). 88% of embryos fail to elongate (n = 41); the remaining 12% of embryos rupture before elongation starts, a more severe phenotype than normally seen in *hmp-1(fe4)* embryos, which only rupture 4% of the time (n = 35). Targeting only the long isoform of MAGI-1 using double-stranded RNA (dsRNA) against the GUK domain only moderately enhances *hmp-1(fe4)* (data not shown). In contrast, targeting both the long and the short isoforms via dsRNA against the third and fourth PDZ motifs significantly enhances *hmp-1(fe4)*. Thus it seems likely that the long isoform alone plays a relatively minor role in synergizing with the CCC during morphogenesis.

To confirm the RNAi phenotype, we attempted to generate a strain carrying *hmp-1(fe4)* and a protein null allele of *magi-1, magi-1(zh66)* [11]; however, we were unable to recover viable progeny. *magi-1(RNAi)* also enhances the penetrance and severity of phenotypes caused by a hypomorphic allele of *hmp-2*β-catenin, *hmp-2(qm39)* [15], and we were able to generate a strain carrying *hmp-2(qm39)* and *magi-1(zh66)*. Embryos from *qm39/qm39; zh66/+* worms exhibited 29.3% lethality (n = 868) and embryos from *qm39/+; zh66/zh66* worms exhibited 39.3% lethality (n = 916). Twenty-five percent of the (presumably) *qm39/qm39; zh66/zh66* embryos ruptured (Figure 1C; Movie S1) and the remaining 75% embryos died at the onset of elongation. That homozygosity for one mutation renders the other haploinsufficient further supports a functional interaction between MAGI-1 and the CCC. Additionally, worms homozygous for either *hmp-2(qm39)* or *magi-1(zh66)* and heterozygous for the other allele had body shape defects, including blunted tails, shortened body length, and midsection bulges.

Loss of MAGI-1 Disrupts Cell Migration Events during Enclosure

Our screen was designed to identify genetic modifiers of CCC-dependent processes during morphogenesis, so we examined ventral enclosure in *magi-1* mutant embryos in more detail [16] (Figure 2). A small number of *magi-1(zh66)* homozygotes

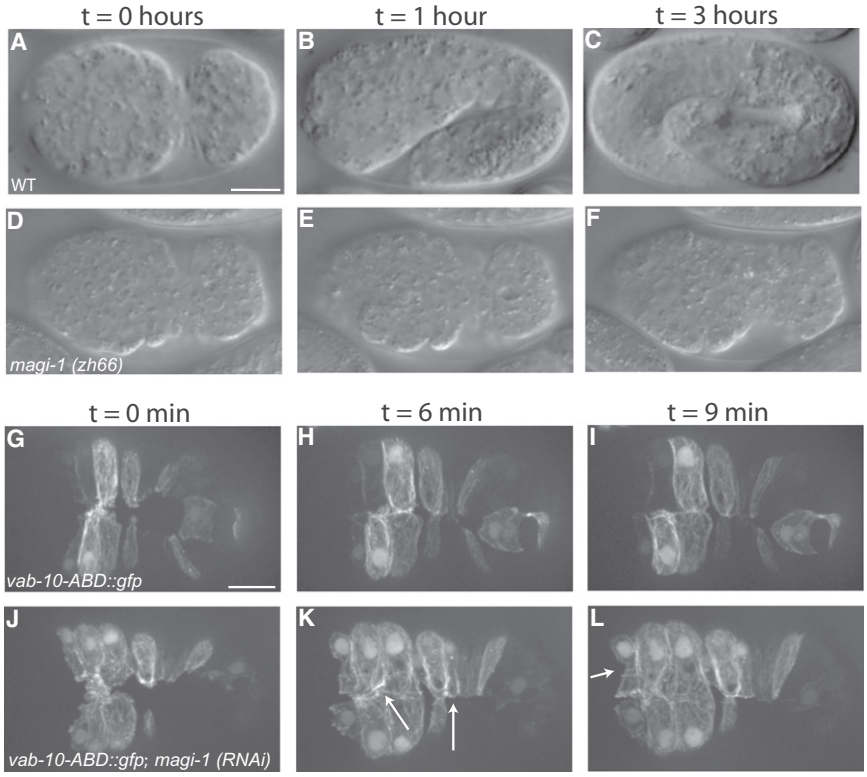

Figure 2. Loss of MAGI-1 Perturbs Ventral Enclosure of the Epidermis

(A–C) WT embryos enclose (A), and elongate (B and C), eventually reaching ~4-fold their original length.

(D–F) A small percentage of embryos homozygous for the null allele *magi-1(zh66)* initiate enclosure (D) but never finish (E and F) and die. Scale bar represents 10 μm.

(G–I) WT embryos expressing an actin reporter during ventral enclosure. During enclosure, cells migrate ventrally, meet their opposing neighbors (G), and form junctions (H) along the ventral midline.

(J–L) In *magi-1(RNAi)* treated embryos, cells still migrate ventrally, but the migration is not as neatly ordered (J). Cells do eventually meet and form junctions, although junctions are often oblique to the ventral midline (arrows, K) and anterior ventral cells often have an irregular shape (arrow, L). Scale bar represents 10 μm.

(1.3%, n = 719; compared to 0.3% lethality, n = 1,130, in WT embryos) arrest during enclosure (Figures 2D–2F; Movie S1). To better understand this phenotype, we performed live imaging of *magi-1(RNAi)* embryos expressing an F-actin reporter [15, 17]. In WT embryos, two pairs of anterior leading cells are the first to extend protrusions ventrally. The cells then meet at the ventral midline, forming nascent junctions (Figure 2G; Movie S2). This behavior continues in more posterior cells (pocket cells), which become wedge-shaped as they elongate toward the ventral midline (Figures 2G and 2H). Finally, anterior epidermal cells encase the anterior-most region of the embryo in epidermis prior to elongation [16] (Figure 2I). In *magi-1(RNAi)* embryos, leading cells extend protrusions, but they often lack directionality and show prolonged protrusive activity (Figure 2J; Movie S2). Although leading cells eventually meet and form junctions, these junctions are not straight along the midline; misalignment also occurs in more posterior ventral cells (Figure 2K, arrows). Finally, in contrast to the rectangular shape seen in WT embryos, anterior ventral cells in *magi-1(RNAi)* embryos often have a more oblong shape (Figure 2L). We observed these defects in 70% of *magi-1* depleted embryos filmed (n = 20) compared to the one WT embryo in which we observed minor defects in (n = 15). These nonuniform cell movements and misalignments of cells at the ventral midline are likely the cause of the morphogenetic failures seen in dead *magi-1(zh66)* embryos.

MAGI-1 Localizes to a Unique Domain in the *C. elegans* Apical Junction

To address the function of MAGI-1, we examined MAGI-1 localization in comma-stage embryos using an antibody that recognizes both isoforms of MAGI-1 [10]. MAGI-1 localizes to cell junctions in all epithelial tissues in *C. elegans*. Triple immunostaining of WT embryos for MAGI-1, HMP-2/β-catenin, and AJM-1 revealed that MAGI-1 localizes basal to the CCC and apical to the DLG-1/AJM-1 complex (n = 7). There was some overlap between the CCC and MAGI-1; however, HMP-2 signal extended more apically than MAGI-1. We also performed pairwise colocalization analysis of MAGI-1 and JAC-1::GFP or AJM-1 separately, which confirmed the results obtained via triple immunolabeling, including the slight overlap between the CCC and MAGI-1 (Figure S1).

SAX-7 Is Important for Localizing MAGI-1 at Junctions

We next assessed effects on junctional localization of MAGI-1 in living embryos when components of the CCC and DLG-1/AJM-1 complex are depleted. MAGI-1::GFP localizes to junctions during epithelial morphogenesis where it persists through development (Figures 3A–3C). We found MAGI-1::GFP is initially targeted to junctions following RNAi-mediated depletion of both HMR-1/cadherin and DLG-1/Discs large, as has been reported in fixed embryos [12]. However, as embryos age, MAGI-1::GFP begins to lose its tight association with junctions (data not shown), indicating that the CCC and DLG-1/AJM-1 complex are not crucial for MAGI-1's initial recruitment but can affect its maintenance at junctions.

To identify transmembrane proteins that initially target MAGI-1 to cell-cell junctions, we targeted 93 previously identified cell adhesion receptors [18] and orthologs of vertebrate transmembrane proteins that bind MAGIs using RNAi and mutants [19–23] (Table S2). We found loss of *sax-7*/L1CAM affected MAGI-1 localization. We crossed *magi-1::gfp* into *sax-7(eq1)* animals and found a reduced amount of MAGI-1::GFP at junctions (Figures 3D–3F; Movie S3). Immunostaining *sax-7(eq1)* embryos for MAGI-1 and AJM-1 showed significantly reduced accumulation of MAGI-1 at junctions (cf. Figures 3H–3J with 3K–3M). We also quantified the apicobasal expression of AJM-1 in *sax-7(eq1)* and *magi-1(zh66)* embryos (556 ± 52 nm, n = 17; 623 ± 51 nm, n = 15, respectively) and found significant expansion compared to WT embryos (421 ± 46 nm, n = 23) (Figure 3N). Although *sax-7* was not found in our feeding screen, injecting dsRNA against *sax-7* into *hmp-1(fe4)* worms did enhance the penetrance and severity of *fe4*

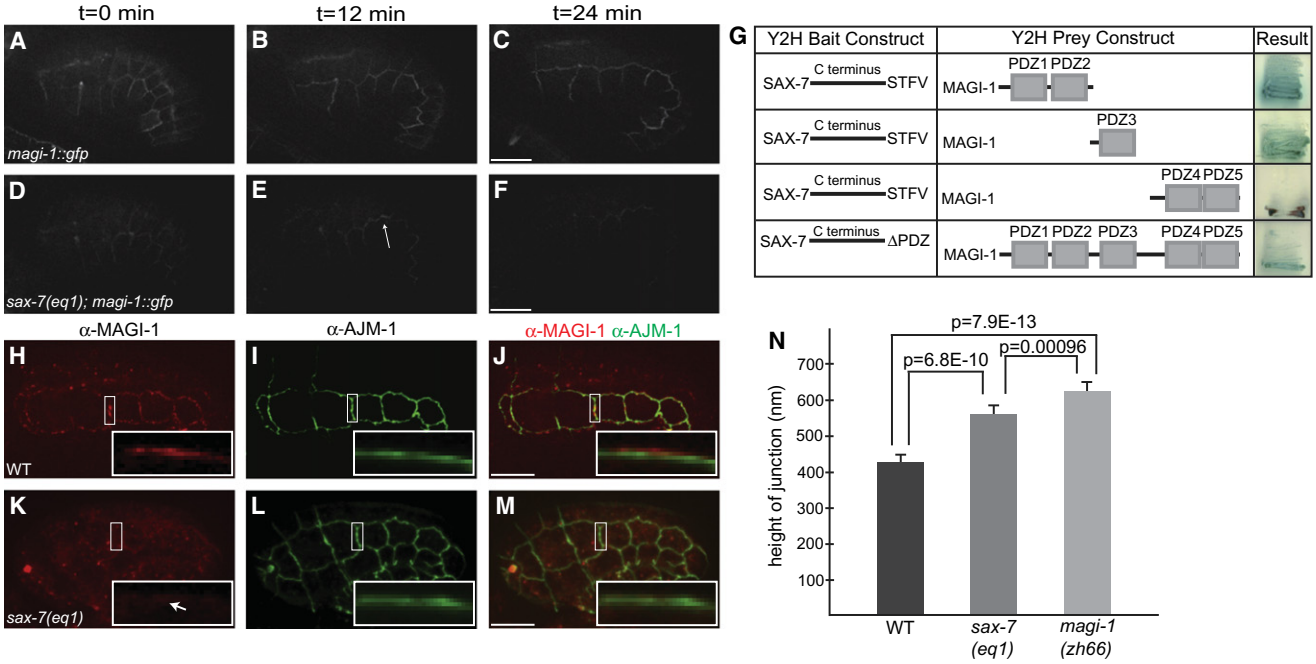

Figure 3. MAGI-1 Localization Partially Depends on SAX-7/L1CAM

(A–C) WT embryos expressing MAGI-1::GFP.

(D–F) The total amount of MAGI-1::GFP at junctions in *sax-7(eq1)* embryos is decreased, but it is not completely absent.

(G) In a directed yeast-two hybrid test, PDZ1-2 and PDZ3 of MAGI-1 can interact with the C terminus of SAX-7, whereas PDZ4-5 of MAGI-1 does not. The ability of MAGI-1 to interact with SAX-7 is reduced when the last four amino acids of SAX-7, a PDZ binding motif, are deleted.

(H–J) In WT embryos, MAGI-1 localizes to junctions (H), apical to AJM-1 (inset, J).

(K–M) In *sax-7(eq1)* embryos, MAGI-1 accumulation is greatly reduced at junctions (white arrow, inset, K) and the region of AJM-1 expression appears expanded (inset, K).

(N) Quantification of the area of AJM-1 expression *sax-7(eq1)* (556 ± 52 nm, mean ± SEM, n = 17) and *magi-1(zh66)* (623 ± 51 nm, n = 15) embryos compared to WT (421 ± 46 nm, n = 23). Significance was calculated using a two-tailed Student's t test. Scale bars represent 10 μm.

phenotypes in a manner similar to depletion of *magi-1* (Figure S2).

We used yeast two-hybrid analysis to test for a physical interaction between MAGI-1's PDZ motifs and the C terminus of SAX-7, which contains a type I consensus PDZ-binding motif [24]. We found that the SAX-7 C terminus was able to bind MAGI-1 PDZ1-2, and PDZ3 and that this interaction was abrogated, although not completely eliminated, by deletion of the SAX-7 PDZ binding motif (Figure 3G). The decrease in junctional accumulation of MAGI-1 in *sax-7* null mutants and the ability of SAX-7 and MAGI-1 to physically interact suggest that SAX-7 is important for recruitment of MAGI-1 to apical junctions.

MAGI-1 Influences the Localization of AFD-1/afadin at Junctions

Because MAGUKs are scaffold proteins [9], we examined the list of screen enhancers to identify potential interacting partners. A promising candidate was AFD-1/afadin/Canoe, an adaptor protein that localizes to cell junctions and can facilitate linkages to the cytoskeleton [25]. Vertebrate afadin can be spliced to produce a shorter variant, AF-6, whose domains—two Ras association (RA1-2) domains, a forkhead-associated (FHA) domain, a Dilute (DIL) domain, a PDZ domain, and a long C terminus with no significant homology—are conserved in *afd-1*. Moreover, *hmp-1(fe4); afd-1(RNAi)* and *hmp-1(fe4); magi-1(RNAi)* treated embryos exhibit similar phenotypes (Figure S2). We used yeast two-hybrid assays to test for an interaction between MAGI-1 and AFD-1. The PDZ domains of MAGI-1 interact with the RA domains and the C terminus of AFD-1, but not a fragment encoding only the DIL-PDZ domains (Figure 4Q).

Based on the yeast two-hybrid interaction, we immunostained WT (Figures 4A–4C), *magi-1(zh66)* (Figures 4D–4F), and *sax-7(eq1)* (Figures 4G–4I) embryos for AFD-1 using affinity purified polyclonal antibodies. AFD-1 accumulates at cell-cell junctions in WT embryos in the epidermis (Figure 4A), pharynx, and intestine (data not shown). We saw dramatically reduced accumulation of AFD-1 at epithelial junctions in both *magi-1(zh66)* and *sax-7(eq1)* embryos (Figures 4D and 4G), indicating that MAGI-1 is important for junctional localization of AFD-1. We also examined the apicobasal position of AFD-1 with respect to AJM-1 and found that, like MAGI-1, AFD-1 was predominantly apical to AJM-1 (data not shown). Reslicing through cell-cell junctions of WT worms expressing MAGI-1::mRFP immunostained for mRFP and AFD-1 revealed a high degree of overlap between the expression patterns of MAGI-1::mRFP and AFD-1 (Figures 4J–4L; Figure 4L, inset).

hmp-1(fe4); magi-1(RNAi) and *hmp-1(fe4); afd-1(RNAi)* Embryos Have a Disorganized Actin Cytoskeleton

afd-1 and *magi-1* both synergize with *hmp-1(fe4)* to predominantly yield elongation failure. Elongation of *C. elegans* embryos depends on a highly organized array of circumferential actin filament bundles, CFBs, which terminate near junctional-proximal accumulations of actin at cell-cell borders

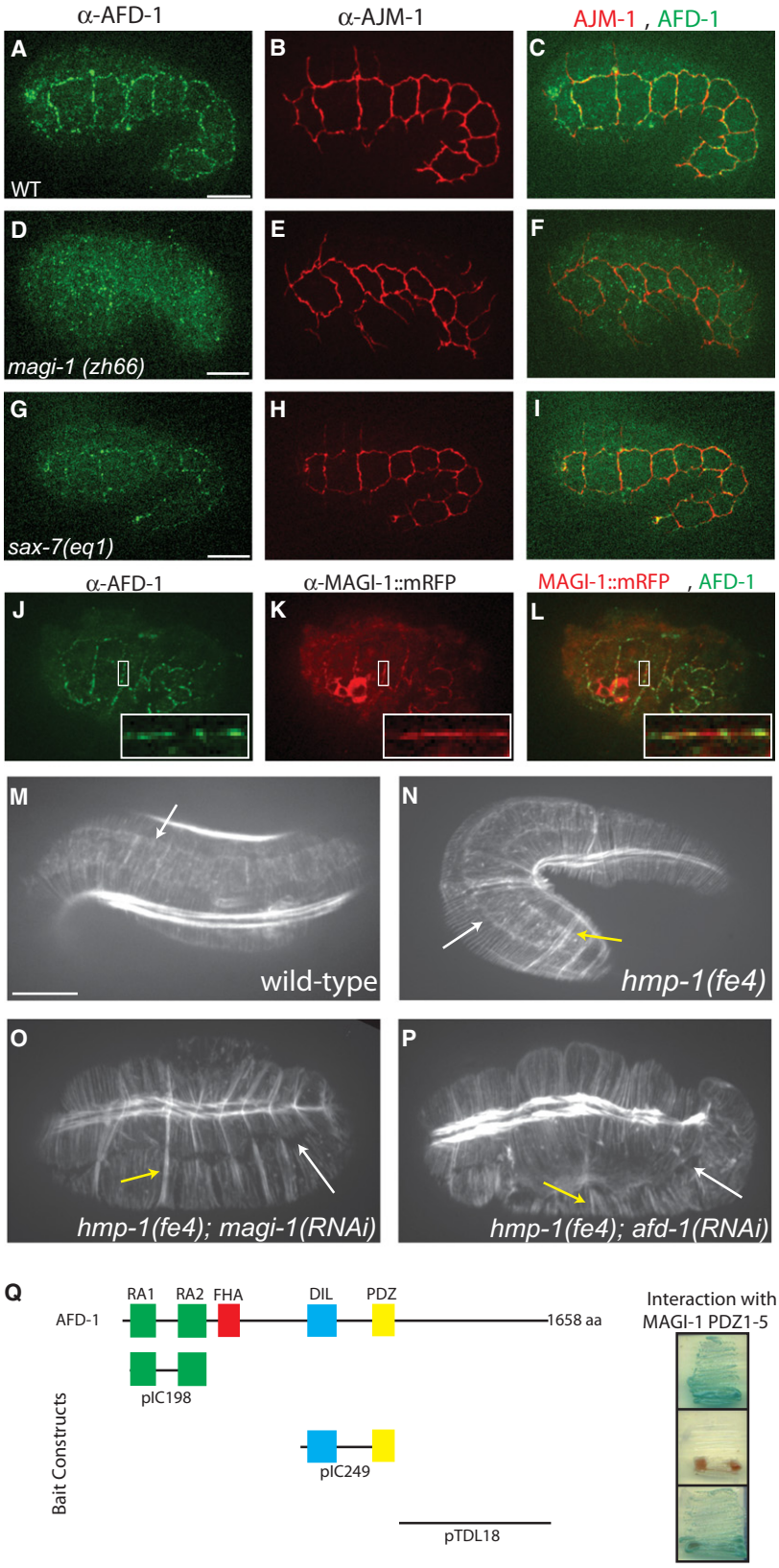

Figure 4. MAGI-1 Influences Localization of AFD-1

(A–C) Immunostaining of AFD-1 in WT embryos shows AFD-1 accumulates at cell junctions (A), but there is little overlap with AJM-1 (C).

(D–F) AFD-1 does not accumulate at cell junctions in *magi-1* null embryos (D), even though AJM-1 still localizes to junctions (E).

(G–I) Consistent with the interaction between SAX-7 and MAGI-1, AFD-1 accumulation at junctions in *sax-7(eq1)* embryos is reduced (G).

(J–L) Immunostaining against MAGI-1::mRFP (K) and AFD-1 (J) reveals a high degree of colocalization between the two proteins (L, inset). Scale bar represents 10 μm.

(M–P) Phalloidin staining of WT embryos shows accumulation of actin and ordered CFBs anchored at the junction (white arrow, M). (N) CFBs in *hmp-1(fe4)* embryos are also anchored at the junction (white arrow); however, some of the CFBs are clumped together (yellow arrow). Similar staining in *hmp-1(fe4); magi-1(RNAi)* (O) and *hmp-1(fe4); afd-1(RNAi)* (P) embryos reveals a loss of junctional proximal actin, and CFBs are completely detached from the junction (white arrows). There are also several clumps of CFBs (yellow arrows). Scale bars represent 10 μm.

(Q) In a directed yeast two-hybrid test, the PDZ domains in MAGI-1 interacted with the RA domains and the C terminus, but not the DIL-PDZ domains of AFD-1.

in epidermal cells [16]. We used phalloidin staining to determine whether AFD-1 or MAGI-1 impacted actin organization during morphogenesis. In WT embryos, CFBs are arranged in parallel arrays anchored at junctions, where there is an accumulation of junctional-proximal actin (Figure 4M). In *hmp-1(fe4)* embryos, junctional-proximal actin is still present and CFBs are still anchored at the junction, but there is some clumping of CFBs (Figure 4N). In *hmp-1(fe4); magi-1(RNAi)* and *hmp-1(fe4); afd-1(RNAi)* embryos, there is also clumping of CFBs; however, CFBs present in these embryos are detached from the junction, and the accumulation of junctional-proximal actin is severely disrupted (Figures 4O and 4P). Because these phenotypes are found in *hmp-1* strong loss-of-function mutants [3], these results suggest MAGI-1 and AFD-1 may modulate the actin cytoskeleton in ways that normally act redundantly with the CCC. To test whether *afd-1* and *magi-1* act in the same or different genetic pathways, we examined *magi-1(zh66); afd-1(RNAi)* embryos. We found a noticeable increase in lethality compared with *magi-1(zh66)* and *afd-1(RNAi)* alone (Figure S2). These results indicate that although the two proteins can physically interact and colocalize, they may act through partially redundant effector pathways.

MAGI-1 Helps to Partition Junctions during Development

The effects of loss of MAGI-1 on adhesion-dependent processes and its position within the apical junction led us to examine potential roles for MAGI-1 in maintaining spatial ordering of apical junctional components, a theory independently suggested in a recent

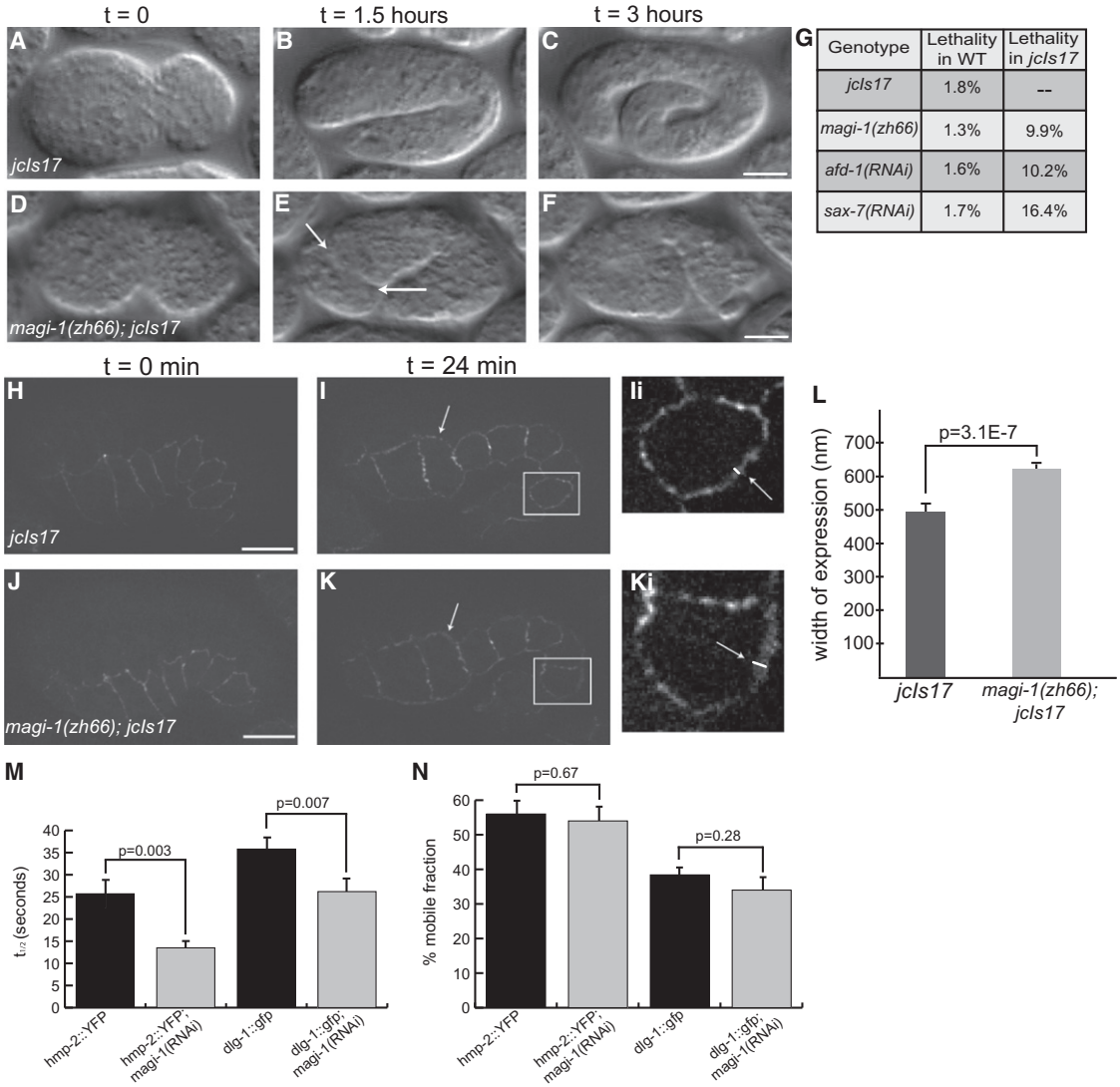

Figure 5. MAGI-1 Helps to Partition Junctions during Development

(A–C) *jcIs17* embryos enclose (A) and elongate as WT embryos do, reaching approximately 4-fold before they hatch (C).

(D–F) *magi-1(zh66); jcIs17* embryos enclose ventrally, but the anterior epidermis does not complete enclosure. When elongation starts, anterior cells spill out of the opening in the epidermis (arrows, E). Scale bars represent 10 μm.

(G) Depleting *magi-1, afd-1* or *sax-7* in *jcIs17* embryos causes similar nonadditive increases in lethality, also primarily due to anterior enclosure defects.

(H–K) At the onset of elongation, *jcIs17* (H) and *magi-1(zh66)*; *jcIs17* (J) embryos look indistinguishable with respect to HMP-1::GFP. As elongation progresses, HMP-1::GFP expression is expanded at seam-dorsal and seam-ventral boundaries in *magi-1(zh66); jcIs17* embryos (arrows, Ii, Ki; white lines indicate width of junctional material). Scale bars represent 10 μm.

(L) *magi-1(zh66); jcIs17* embryos exhibit an expanded area of HMP-1::GFP expression (618 ± 29 nm, mean ± SEM, n = 10) in seam cells compared to WT embryos (493 ± 49 nm, n = 13). Significance was calculated using a two-tailed Student's t test.

(M) *magi-1(RNAi)* decreases the half-life ($t_{1/2}$) of fluorescence recovery after photobleaching in embryos expressing *hmp-2::yfp* or *dlg-1::gfp*.

(N) *magi-1(RNAi)* does not significantly affect the mobile fraction of either HMP-2::YFP or DLG-1::GFP.

study [12]. We hypothesized that overexpression of members of apical junctional complexes might lead to more severe phenotypes when MAGI-1 is absent. We therefore generated the strain *zh66/zh66; jcIs17* [*Phmp-1::hmp-1::gfp, Pdlg-1::dlg-1::dsRed*]. In contrast to *magi-1(zh66)* and *jcIs17* embryos (Figures 5A–5C), which each display a small amount of lethality (1%–2%), depleting *magi-1* in *jcIs17* worms results in ~10% embryonic lethality that is predominantly due to enclosure failure (Figures 5D–5F and 5G; Movie S4). This lethality is most likely due to overexpression of junctional proteins because *gfp(RNAi)* reduced the lethality in *zh66; jcIs17* embryos to 3.25% (n = 660). We also knocked down *sax-7* and *afd-1* in *jcIs17* worms and found similar increase in lethality (Figure 5G). These phenotypic similarities provide further evidence that MAGI-1, SAX-7, and AFD-1 can act together during morphogenesis in *C. elegans* embryos.

We filmed *magi-1(zh66); jcIs17* embryos to analyze their defects. During enclosure and at the comma stage, HMP-1::GFP is evenly distributed along junctions; localization does not change significantly at the 1.5-fold stage in *jcIs17* embryos (Figures 5H, 5I, and 5Ii). *magi-1(zh66); jcIs17* embryos look indistinguishable from *jcIs17* embryos during

enclosure through the comma stage (Figure 5J). However, at the 1.5-fold stage, just before embryos start to elongate, *magi-1(zh66); jcIs17* embryos display an expanded area of HMP-1::GFP expression at the borders between lateral (seam) and ventral epidermal cells and at seam-dorsal borders (Figures 5K and 5Ki). We quantified the expansion of HMP-1::GFP width and found a significant increase in *magi-1(zh66); jcIs17* embryos compared to *jcIs17* embryos (Figure 5L).

Previous work has shown apical junction formation occurs in two steps: assembly, during which proteins are targeted to the membrane, and establishment, when junctions segregate into compact domains along the apicobasal axis that are maintained throughout development [5]. Because enclosure and comma stage *jcIs17* and *zh66/zh66*; *jcIs17* embryos look indistinguishable, our results are consistent with a role for MAGI-1 in spatial compaction of the apical junction or maintenance of its compacted state. Loss of compaction may in turn weaken cell-cell adhesion.

In addition to aiding apicobasal compaction of the apical junction, MAGI-1 could also stabilize junctional components by restricting their movement. To address this question, we examined the mobility of junctional proteins in WT and *magi-1(RNAi)* treated embryos using fluorescence recovery after photobleaching (FRAP). In *hmp-2::yfp* embryos, depleting MAGI-1 significantly reduced the half-life of recovery after photobleaching, $t_{1/2}$, from 25.7 ± 6.2 s to 13.5 ± 2.8 s (n = 6, significantly different in a two-tailed Student's t test, p = 0.003) (Figure 5M). In *dlg-1::gfp* embryos, *magi-1(RNAi)* significantly reduced the half-life of recovery from $t_{1/2}$ = 35.8 ± 5.1 s to $t_{1/2}$ = 26.2 ± 5.6 s (n = 6, p = 0.007) (Figure 5M). *magi-1(RNAi)* treatment did not significantly change the percent mobile fraction for either protein (*hmp-2::yfp* versus *hmp-2::yfp; magi-1(RNAi)*: 56% ± 7.4% versus 54% ± 7.8%, n = 6, p = 0.673; *dlg-1::gfp* versus *dlg-1::gfp; magi-1(RNAi)*: 38.4% ± 4% versus 34% ± 7.3%, n = 6, p = 0.28) (Figure 5N). These results suggest that MAGI-1 normally stabilizes proteins once they arrive and assemble at the apical junction.

Discussion

An Enhancer Screen Identifies Putative Adhesion Modulators during *C. elegans* Morphogenesis

C. elegans is a useful system for identifying additional conserved modulators of cell-cell adhesion in metazoans [2]. Because forward genetic approaches do not always identify modifiers or redundant genes, we used genome-wide RNAi in a hypomorphic *hmp-1*/α-catenin mutant background to uncover 55 novel regulators of cell junctions in vivo. We focused on *magi-1*, a critical regulator of junctional stability in vertebrate tissue culture [26, 27]. We subsequently confirmed the genetic interaction between *magi-1* and the CCC using *magi-1* and *hmp-2*/β-catenin mutants, providing further support for their functional interaction.

Our screen also identified the junctional proteins *jac-1*/p120-catenin [14], *zoo-1*/ZO-1 [15], and *srgp-1*/srGAP [28], whose synergy with *hmp-1(fe4)* we have previously reported. Additionally, we identified cytoskeletal modulators including *unc-34*/Enabled [29], TMD-1/tropomodulin [30], and FLI-1/Flightless, which has been implicated in numerous nonepithelial processes in *C. elegans* [31]. We also identified proteins involved in vesicular trafficking. These include a component of the exocyst complex (SEC-8) and components of the AP-2 clathrin adaptor complex (APS-2, APA-2), which could be involved in trafficking CCC components. We also found genes involved in protein turnover, including EEL-1, an E3 ligase that has been implicated in indirect regulation of hemidesmosome-like structures in *C. elegans* [32]. In summary, our screen is the first genome-wide approach to identifying proteins that act alongside the CCC during morphogenesis and should provide the basis for future experiments to clarify the roles of the CCC interactome during morphogenesis.

MAGI-1 Aids Collective Cell Migration during Epidermal Morphogenesis

We identified a role for MAGI-1 in modulating cell-cell contact during ventral enclosure, consistent with work in vertebrate tissue culture, where loss of MAGI-1 weakens cell-cell adhesion, leading to dismantling of cell junctions [26, 27]. Loss of *C. elegans magi-1* function could similarly weaken cell junctions, thereby impairing normal coordination of cell movements during ventral enclosure. Because defects in anterior epidermal cell migration occur before contralateral cells make nascent junctional connections, the nonuniform shape of ventral cells during enclosure may reflect weakened adhesion along lateral edges of cells when MAGI-1 is absent. Similarly, overreaching of contralateral cells at the ventral midline may reflect lack of suppression of motility upon ventral midline contact. Similar defects in collective cell migration have been observed in cultured cells during healing of scratch wounds in the presence of function-blocking anti-E-cadherin antibodies [33].

MAGI-1 Localizes between the CCC and the DLG-1/AJM-1 Complex at the Junction

Although MAGI-1 had been reported to be at cell-cell junctions [10], we determined that MAGI-1 localizes to a unique junctional domain between the CCC and the DLG-1/AJM-1 complex. Our results are contrast with a recent paper that placed MAGI-1 apical to both the CCC and the DLG-1/AJM-1 complex [12]. This difference could possibly be due to localization differences between endogenous MAGI-1, which we examined in our antibody staining experiments, and fluorescently tagged MAGI-1, used in the previous study. The embryo presented in [12] was also significantly older than the embryos examined here; however, we examined embryos of various ages and found no changes in apicobasal ordering of proteins at the apical junction as development proceeded. Our results are internally consistent and reflect numerous permutations of pairwise and triple labeling.

Localization of MAGI-1 to Junctions Partly Depends on SAX-7/L1CAM

We failed to find any candidates whose removal completely prevented localization of MAGI-1 at junctions. This is not surprising because multiple domains of the protein are sufficient to target it to junctions [12]. We did, however, see significant effects on MAGI-1 localization due to loss of *sax-7* function. A yeast two-hybrid assay further demonstrated that SAX-7 and MAGI-1 can physically interact, suggesting that localization of MAGI-1 to junctions depends in part on SAX-7 binding. The expanded area of expression of AJM-1 in *sax-7* null embryos relative to WT also supports this view, because expansion of the DLG-1/AJM-1 complex had been previously demonstrated in *magi-1* null embryos [12].

MAGI-1 Interacts Downstream with AFD-1/afadin/AF6 and Regulates the Actin Cytoskeleton at Junctions

We showed that MAGI-1 and AFD-1, another screen enhancer, can interact in a directed yeast two-hybrid assay via the RA domains and the C terminus of AFD-1. Moreover, AFD-1 localization is significantly disrupted in *magi-1* null embryos. Importantly, *afd-1(RNAi)* has no discernable effect on the ability of MAGI-1::GFP to localize to junctions (data not shown). To our knowledge, this is the first report linking MAGI-1 and AFD-1/afadin. Afadin has previously been linked to ZO-1, another MAGUK, in both vertebrates and *Drosophila* [34, 35], but not to MAGIs. Although we cannot rule out an interaction between AFD-1 and the *C. elegans* ZO ortholog, ZOO-1, our antibody staining shows that AFD-1 and MAGI-1 colocalize at cell junctions, whereas ZOO-1 localizes predominantly with the CCC [15]. We conclude that AFD-1 and MAGI-1 are part of the same junctional subdomain.

The disorganized actin phenotypes seen in both *hmp-1(fe4); magi-1(RNAi)* and *hmp-1(fe4); afd-1(RNAi)* embryos raise the possibility that MAGI-1 influences the actin cytoskeleton through AFD-1. Because MAGI-1 and AFD-1 are spatially distinct from the CCC, our results further suggest that MAGI-1 and AFD-1 modulate the actin cytoskeleton in ways that normally act redundantly with the CCC. Although the *C. elegans* afadin ortholog is missing a conserved actin-binding domain at the C terminus, the remainder of the C terminus is intact, so it is possible that the AFD-1 C terminus can interact with actin. AFD-1 also possesses two RA domains, which are capable of interacting with Rap1, a known cytoskeletal modulator in other systems [36]. Knocking down either *magi-1* or *afd-1* could affect RAP activity at junctions, contributing to the actin organization defects seen in *hmp-1(fe4); magi-1(RNAi)* and *hmp-1(fe4); afd-1(RNAi)* embryos. Determining whether AFD-1 can bind actin and interact with RAPs could address these possibilities in the future.

MAGI-1 May Act to Separate the CCC and DLG-1/AJM-1 Complexes

A recent paper suggested that MAGI-1 has a role in maintaining the spatial separation of complexes at the apical junction [12]. Our examination of fluorescent protein expression in *magi-1* null mutants overexpressing HMP-1 and DLG-1 supports this experimentally. HMP-1::GFP expression was expanded at seam-ventral and seam-dorsal boundaries in 1.5-fold *magi-1* null embryos, immediately before embryos commence elongation, but not during enclosure, when nascent junctions are being formed. Elongation places stress on cell junctions, as the contractile forces are transmitted to CFBs anchored at epidermal cell-cell junctions. The expansion of the domain containing HMP-1::GFP in *magi-1(zh66)* embryos suggests that loss of *magi-1* causes a weakening of junctions at this time. Our FRAP analysis further supports this idea. The increased rates of recovery after photobleaching in embryos expressing either DLG-1::GFP or HMP-2::YFP following *magi-1* knockdown suggest that once they are incorporated into mature junctions, MAGI-1 may stabilize both the CCC and DLG-1/AJM-1 complex proteins.

Given its localization between the two complexes in our hands, MAGI-1 may separate the two complexes and stabilize them into a more structurally rigid complex. This model is consistent with the expansion of AJM-1 expression in *sax-7* null embryos, the expansion of HMP-1::GFP in *magi-1* null embryos, and the mixing of junctional complexes previously reported by others [12]. It also explains the increases in lethality seen in *jcIs17* embryos, which overexpress HMP-1::GFP and DLG-1::dsRed, following knockdown of *magi-1*, *sax-7*, or *afd-1*. Excess proteins from the two complexes may further exacerbate mixing of the two subdomains, further disorganizing the junction.

Conclusion

We have performed the first genome-wide functional screen for proteins that act alongside the CCC during morphogenesis. MAGI-1, along with SAX-7/L1CAM and AFD-1/afadin, are part of a functional interactome that includes the core CCC. We favor a model in which MAGI-1 serves as a partition between the CCC and DLG-1/AJM-1 complex, acting both to keep the complexes spatially separated and to stabilize them into a more rigid structure.

Our results also suggest that MAGI-1 is anchored at the plasma membrane in part through an interaction with SAX-7. A connection to the actin cytoskeleton via AFD-1 could stabilize the MAGI-1 partition at its cytoplasmic interface. Such a connection to the actin cytoskeleton could act in parallel to HMP-1, which could explain the enhancement of *hmp-1(fe4)* we see following loss of function for either *magi-1* or *afd-1*. Our results expand our understanding of the in vivo roles of MAGI-1 in cell-cell adhesion, and underscore the utility of *C. elegans* as a model system for identifying conserved components of a functionally interacting network of proteins that facilitate cell-cell adhesion in a living embryo.

Supplemental Information

Supplemental Information includes three figures, two tables, Supplemental Experimental Procedures, and four movies and can be found with this article online at http://dx.doi.org/10.1016/j.cub.2012.08.024.

Acknowledgments

This work was supported by National Institutes of Health (NIH) grant R01 GM58038 to J.H., a genetics program predoctoral training grant NIH 5T32GM07133 to A.M.L., NIH grant NRSA GM067410 and grant R15 HD059952 to E.C.-P., and an American Cancer Society Postdoctoral Fellowship awarded to T.G. We thank Yuji Kohara for providing complementary DNAs, A. Stetak (University of Basel) for sharing the MAGI-1::GFP and HMP-2::YFP strains. T. Loveless (University of Wisconsin) and L. Chen (University of Minnesota) for providing Y2H constructs, and C. Rongo (Rutgers University) for the MAGI-1 antibody.

Received: February 14, 2012
Revised: July 20, 2012
Accepted: August 14, 2012
Published online: September 13, 2012

References

1. Niessen, C.M., Leckband, D., and Yap, A.S. (2011). Tissue organization by cadherin adhesion molecules: dynamic molecular and cellular mechanisms of morphogenetic regulation. Physiol. Rev. *91*, 691–731.
2. Lynch, A.M., and Hardin, J. (2009). The assembly and maintenance of epithelial junctions in C. elegans. Front. Biosci. *14*, 1414–1432.
3. Costa, M., Raich, W., Agbunag, C., Leung, B., Hardin, J., and Priess, J.R. (1998). A putative catenin-cadherin system mediates morphogenesis of the Caenorhabditis elegans embryo. J. Cell Biol. *141*, 297–308.
4. Köppen, M., Simske, J.S., Sims, P.A., Firestein, B.L., Hall, D.H., Radice, A.D., Rongo, C., and Hardin, J.D. (2001). Cooperative regulation of AJM-1 controls junctional integrity in Caenorhabditis elegans epithelia. Nat. Cell Biol. *3*, 983–991.
5. McMahon, L., Legouis, R., Vonesch, J.L., and Labouesse, M. (2001). Assembly of C. elegans apical junctions involves positioning and compaction by LET-413 and protein aggregation by the MAGUK protein DLG-1. J. Cell Sci. *114*, 2265–2277.

6. Heasman, J., Ginsberg, D., Geiger, B., Goldstone, K., Pratt, T., Yoshida-Noro, C., and Wylie, C. (1994). A functional test for maternally inherited cadherin in Xenopus shows its importance in cell adhesion at the blastula stage. Development *120*, 49–57.
7. Larue, L., Ohsugi, M., Hirchenhain, J., and Kemler, R. (1994). E-cadherin null mutant embryos fail to form a trophectoderm epithelium. Proc. Natl. Acad. Sci. USA *91*, 8263–8267.
8. Müller, H.A., and Wieschaus, E. (1996). armadillo, bazooka, and stardust are critical for early stages in formation of the zonula adherens and maintenance of the polarized blastoderm epithelium in Drosophila. J. Cell Biol. *134*, 149–163.
9. Funke, L., Dakoji, S., and Bredt, D.S. (2005). Membrane-associated guanylate kinases regulate adhesion and plasticity at cell junctions. Annu. Rev. Biochem. *74*, 219–245.
10. Emtage, L., Chang, H., Tiver, R., and Rongo, C. (2009). MAGI-1 modulates AMPA receptor synaptic localization and behavioral plasticity in response to prior experience. PLoS ONE *4*, e4613.
11. Stetak, A., Hörndli, F., Maricq, A.V., van den Heuvel, S., and Hajnal, A. (2009). Neuron-specific regulation of associative learning and memory by MAGI-1 in C. elegans. PLoS ONE *4*, e6019.
12. Stetak, A., and Hajnal, A. (2011). The C. elegans MAGI-1 protein is a novel component of cell junctions that is required for junctional compartmentalization. Dev. Biol. *350*, 24–31.
13. Kamath, R.S., and Ahringer, J. (2003). Genome-wide RNAi screening in Caenorhabditis elegans. Methods *30*, 313–321.
14. Pettitt, J., Cox, E.A., Broadbent, I.D., Flett, A., and Hardin, J. (2003). The Caenorhabditis elegans p120 catenin homologue, JAC-1, modulates cadherin-catenin function during epidermal morphogenesis. J. Cell Biol. *162*, 15–22.
15. Lockwood, C., Zaidel-Bar, R., and Hardin, J. (2008). The C. elegans zonula occludens ortholog cooperates with the cadherin complex to recruit actin during morphogenesis. Curr. Biol. *18*, 1333–1337.
16. Chisholm, A.D., and Hardin, J. (2005). Epidermal morphogenesis. WormBook, 1–22. http://dx.doi.org/10.1895/wormbook.1.35.1.
17. Gally, C., Wissler, F., Zahreddine, H., Quintin, S., Landmann, F., and Labouesse, M. (2009). Myosin II regulation during C. elegans embryonic elongation: LET-502/ROCK, MRCK-1 and PAK-1, three kinases with different roles. Development *136*, 3109–3119.
18. Cox, E.A., Tuskey, C., and Hardin, J. (2004). Cell adhesion receptors in C. elegans. J. Cell Sci. *117*, 1867–1870.
19. Xu, Z., Peng, A.W., Oshima, K., and Heller, S. (2008). MAGI-1, a candidate stereociliary scaffolding protein, associates with the tip-link component cadherin 23. J. Neurosci. *28*, 11269–11276.
20. Hirabayashi, S., Tajima, M., Yao, I., Nishimura, W., Mori, H., and Hata, Y. (2003). JAM4, a junctional cell adhesion molecule interacting with a tight junction protein, MAGI-1. Mol. Cell. Biol. *23*, 4267–4282.
21. Wegmann, F., Ebnet, K., Du Pasquier, L., Vestweber, D., and Butz, S. (2004). Endothelial adhesion molecule ESAM binds directly to the multidomain adaptor MAGI-1 and recruits it to cell contacts. Exp. Cell Res. *300*, 121–133.
22. Patrie, K.M., Drescher, A.J., Goyal, M., Wiggins, R.C., and Margolis, B. (2001). The membrane-associated guanylate kinase protein MAGI-1 binds megalin and is present in glomerular podocytes. J. Am. Soc. Nephrol. *12*, 667–677.
23. Ide, N., Hata, Y., Nishioka, H., Hirao, K., Yao, I., Deguchi, M., Mizoguchi, A., Nishimori, H., Tokino, T., Nakamura, Y., and Takai, Y. (1999). Localization of membrane-associated guanylate kinase (MAGI)-1/BAI-associated protein (BAP) 1 at tight junctions of epithelial cells. Oncogene *18*, 7810–7815.
24. Zhou, S., Opperman, K., Wang, X., and Chen, L. (2008). unc-44 Ankyrin and stn-2 gamma-syntrophin regulate sax-7 L1CAM function in maintaining neuronal positioning in Caenorhabditis elegans. Genetics *180*, 1429–1443.
25. Sawyer, J.K., Harris, N.J., Slep, K.C., Gaul, U., and Peifer, M. (2009). The Drosophila afadin homologue Canoe regulates linkage of the actin cytoskeleton to adherens junctions during apical constriction. J. Cell Biol. *186*, 57–73.
26. Gregorc, U., Ivanova, S., Thomas, M., Guccione, E., Glaunsinger, B., Javier, R., Turk, V., Banks, L., and Turk, B. (2007). Cleavage of MAGI-1, a tight junction PDZ protein, by caspases is an important step for cell-cell detachment in apoptosis. Apoptosis *12*, 343–354.
27. Kranjec, C., and Banks, L. (2010). A systematic analysis of HPV E6 PDZ substrates identifies MAGI-1 as a major target of HPV-16 and HPV-18 whose loss accompanies disruption of Tight Junctions. J. Virol. *85*, 1757–1764.
28. Zaidel-Bar, R., Joyce, M.J., Lynch, A.M., Witte, K., Audhya, A., and Hardin, J. (2010). The F-BAR domain of SRGP-1 facilitates cell-cell adhesion during C. elegans morphogenesis. J. Cell Biol. *191*, 761–769.
29. Sheffield, M., Loveless, T., Hardin, J., and Pettitt, J. (2007). C. elegans Enabled exhibits novel interactions with N-WASP, Abl, and cell-cell junctions. Curr. Biol. *17*, 1791–1796.
30. Cox-Paulson, E.A., Walck-Shannon, E., Lynch, A.M., Yamashiro, S., Zaidel-Bar, R., Eno, C.C., Ono, S., and Hardin, J. (2012). Tropomodulin Protects α-Catenin-Dependent Junctional-Actin Networks under Stress during Epithelial Morphogenesis. Curr. Biol. Published online July 3, 2012. http://dx.doi.org/10.1016/j.cub.2012.06.025.
31. Deng, H., Xia, D., Fang, B., and Zhang, H. (2007). The Flightless I homolog, fli-1, regulates anterior/posterior polarity, asymmetric cell division and ovulation during Caenorhabditis elegans development. Genetics *177*, 847–860.
32. Zahreddine, H., Zhang, H., Diogon, M., Nagamatsu, Y., and Labouesse, M. (2010). CRT-1/calreticulin and the E3 ligase EEL-1/HUWE1 control hemidesmosome maturation in C. elegans development. Curr. Biol. *20*, 322–327.
33. Lorger, M., and Moelling, K. (2006). Regulation of epithelial wound closure and intercellular adhesion by interaction of AF6 with actin cytoskeleton. J. Cell Sci. *119*, 3385–3398.
34. Takahashi, K., Matsuo, T., Katsube, T., Ueda, R., and Yamamoto, D. (1998). Direct binding between two PDZ domain proteins Canoe and ZO-1 and their roles in regulation of the jun N-terminal kinase pathway in Drosophila morphogenesis. Mech. Dev. *78*, 97–111.
35. Yamamoto, T., Harada, N., Kano, K., Taya, S., Canaani, E., Matsuura, Y., Mizoguchi, A., Ide, C., and Kaibuchi, K. (1997). The Ras target AF-6 interacts with ZO-1 and serves as a peripheral component of tight junctions in epithelial cells. J. Cell Biol. *139*, 785–795.
36. Kooistra, M.R., Dubé, N., and Bos, J.L. (2007). Rap1: a key regulator in cell-cell junction formation. J. Cell Sci. *120*, 17–22.
37. Cram, E.J., Shang, H., and Schwarzbauer, J.E. (2006). A systematic RNA interference screen reveals a cell migration gene network in C. elegans. J. Cell Sci. *119*, 4811–4818.
38. Kamath, R.S., Fraser, A.G., Dong, Y., Poulin, G., Durbin, R., Gotta, M., Kanapin, A., Le Bot, N., Moreno, S., Sohrmann, M., et al. (2003). Systematic functional analysis of the Caenorhabditis elegans genome using RNAi. Nature *421*, 231–237.

Current Biology, Volume *22*

Supplemental Information

A Genome-wide Functional Screen Shows MAGI-1 Is an L1CAM-Dependent Stabilizer of Apical Junctions in *C. elegans*

Allison M. Lynch, Theresa Grana, Elisabeth Cox-Paulson, Annabelle Couthier, Michel Cameron, Ian Chin-Sang, Jonathan Pettitt, and Jeff Hardin

Supplemental Inventory

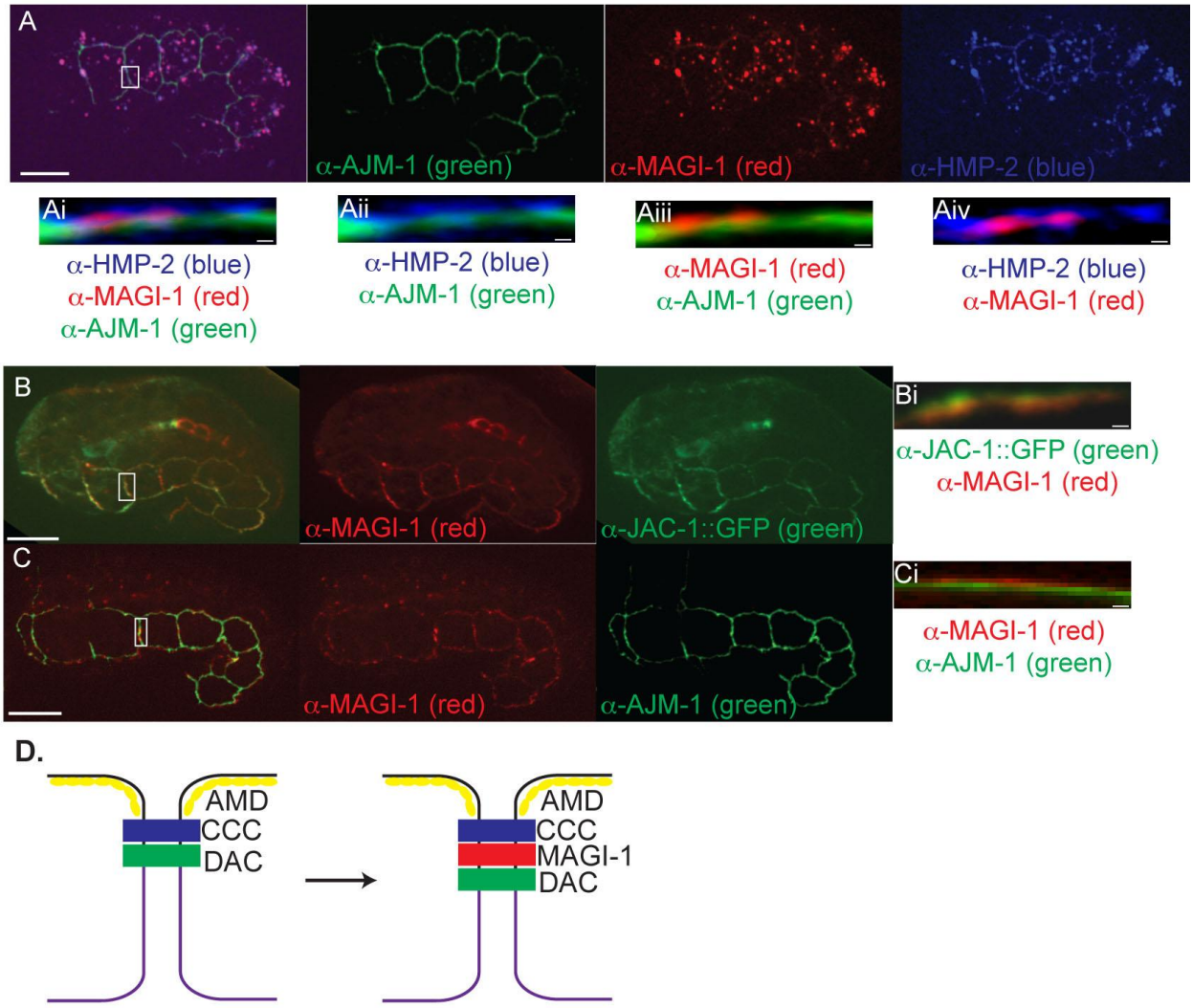

Figure S1. MAGI-1 Localizes to a Unique Junctional Domain and Helps Regulate Enclosure, Related to Figure 3

Wild type embryos immunostained for HMP-2, MAGI-1, and AJM-1 (A), JAC-1::GFP and MAGI-1 (B), and MAGI-1 and AJM-1 (C). Junctions were examined using Volocity (A, Bi) and ImageJ (Ci). MAGI-1 does not primarily colocalize with the cadherin-catenin complex (CCC), or the DLG-1/AJM-1 complex (DAC), but rather resides between them, although there is some overlap between MAGI-1 and the CCC. A, B, C scale bar = 10μm. Ai-iv, Bi, Ci scale bar = 0.5μm. (D) Schematic of the *C. elegans* apical junction to include MAGI-1.

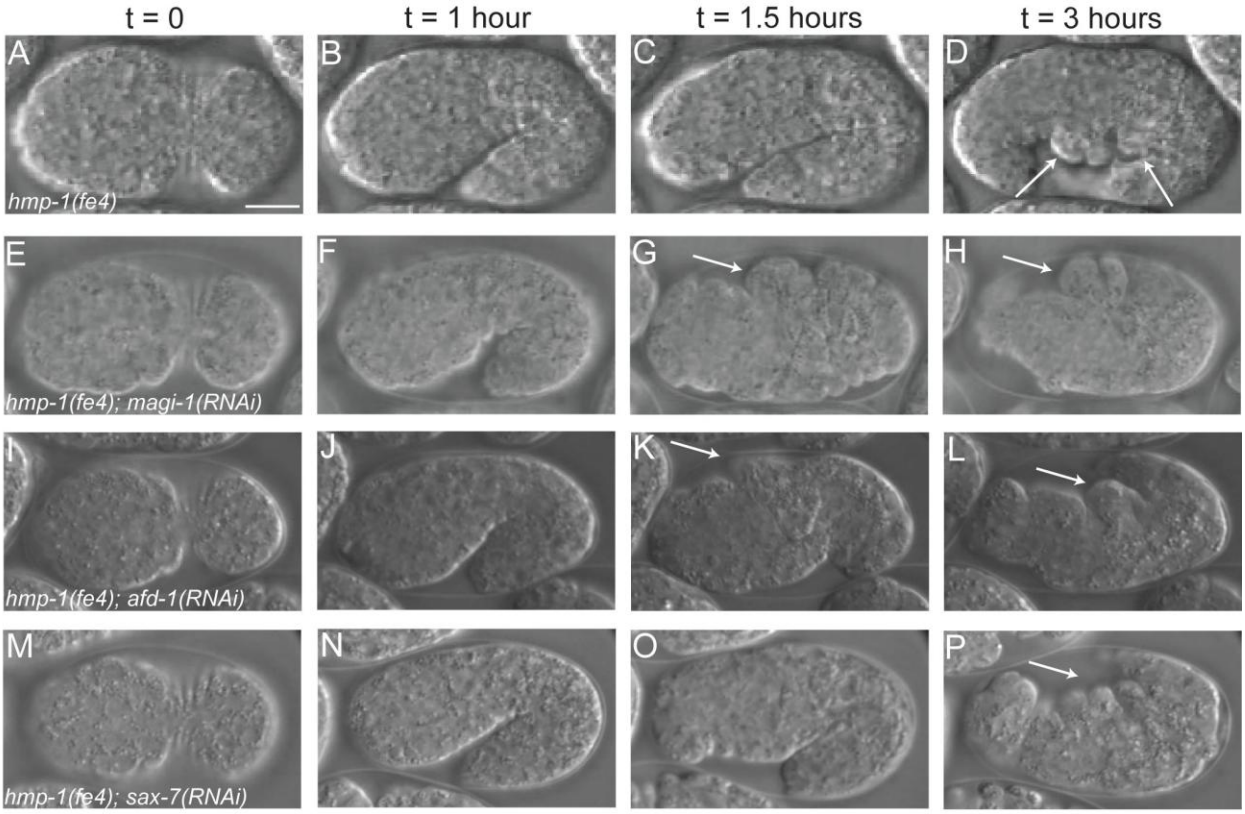

Figure S2. *hmp-1(fe4)* Phenotypes Are Enhanced Similarly by Depletion of *magi-1*, *afd-1*, or *sax-7*, Related to Figures 3 and 4

(A-D) *hmp-1(fe4)* embryos enclose (A), but fail to fully elongate, developing body shape defects (arrow, D). The majority of *hmp-1(fe4)*; *magi-1(RNAi)* (E), *hmp-1(fe4); afd-1(RNAi)* (I), and *hmp-1(fe4); sax-7(RNAi)* (M) embryos enclose, but almost immediately retract dorsally and arrest, with a characteristic humpback phenotype (arrows). Scale bar = 10 μm.

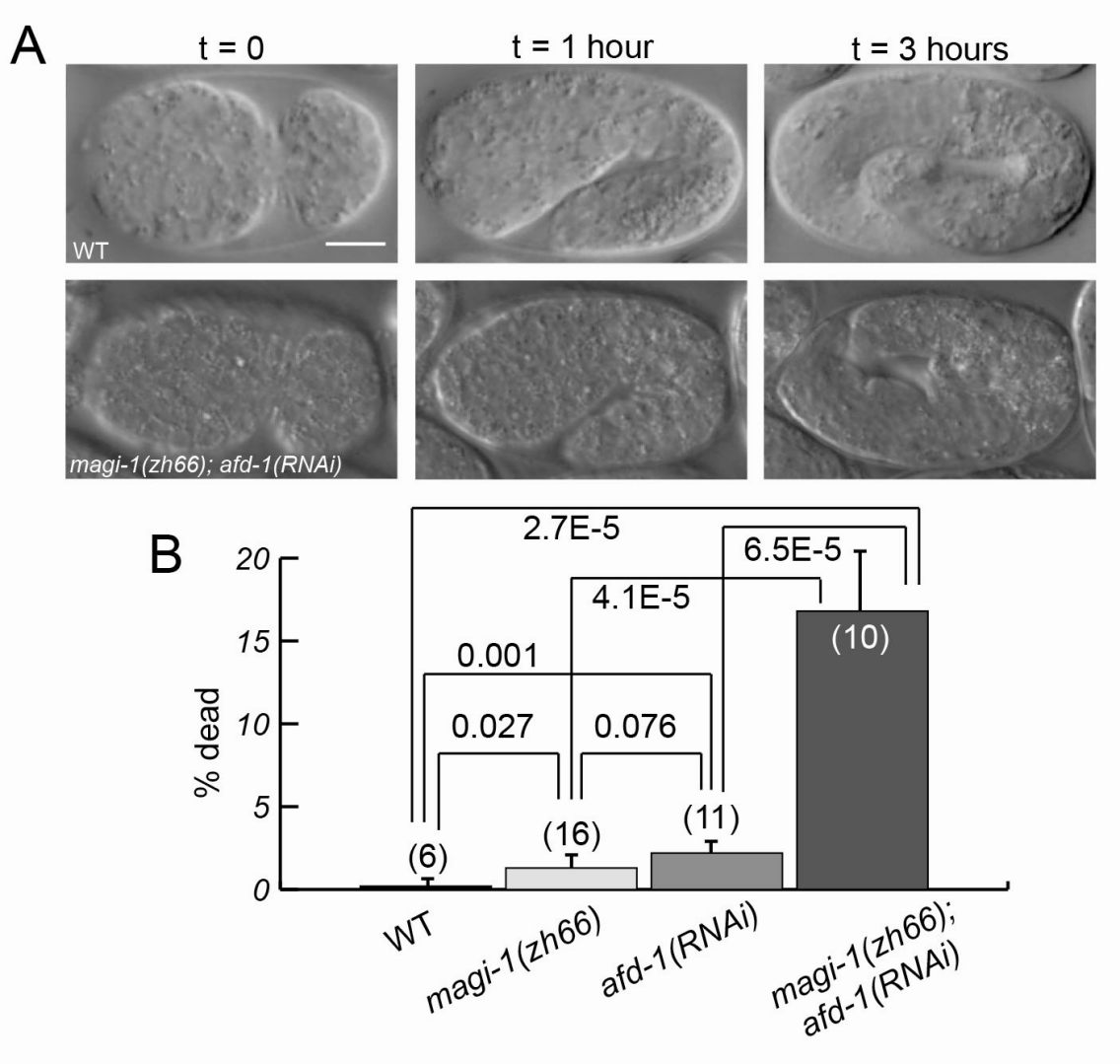

Figure S3. *afd-1(RNAi)* Enhances the Lethality of *magi-1(zh66)*, Related to Figure 4

(A) Synergistic defects in *magi-1(zh66); afd-1(RNAi)* embryos. Wild-type embryos enclose (t = 0), turn (t = 1 hour), and elongate ~4-fold their original length before hatching (t = 3 hours). Some *magi-1(zh66); afd-1(RNAi)* embryos still enclose (t=0), but fail to elongate properly, developing body morphology defects (t=3 hours). Scale bar = 10 μm.

(B) Quantification of defects in *afd-1; magi-1* loss of function embryos. Bars = mean ± SEM; (n) = number of worms whose progeny were scored. p values for pairwise comparisons are shown.

Table S1. *hmp-1(fe4)* Enhancers Identified in a Genome Wide Feeding RNAi Screen, Related to Figure 1

Gene	Protein	N2 lethality	*hmp-1(fe4)* lethality	Terminal phenotype
Y105C5B.21	JAC-1	0%	100%	Severe elongation defect
Y105E8A.26	ZOO-1	0%	100%	Moderate elongation defect
Y50D4C.1	UNC-34	0%	100%	Moderate elongation defect
C06A5.7	TMD-1	7.5%	100%	Severe elongation defect
W03F11.6	AFD-1	6.4%	100%	Severe elongation defect
M01E5.5	TOP-1	5.5%	100%	Elongation defect
F29D11.2	CAPG-1	10.0%	100%	Elongation defect
G46A9.6	MEC-8	11.8%	100%	Elongation defect
C10G11.7	unknown	10.6%	99.6%	Elongation defect
Y106G6H.7	SEC-8	4.3%	97.9%	Elongation defect
R05D7.5	unknown	7.8%	96.1%	Elongation defect
F10E7.8	FARL-11	2.9%	99.5%	Severe/moderate elongation defect
C41C4.6	ULP-4	3.0%	98.7%	Severe elongation defect
CO8H9.2	unknown	0.0%	100%	Moderate elongation defect
C06A1.1	CDC-48.1	1.5%	96.6%	Gastrulation defect
Y48C3A.8	SAM-1	0.4%	88.4%	Moderate elongation defect
B0523.5	FLI-1	0.0%	100%	Severe elongation defect
B0303.9	VPS-33.1	0.5%	88.7%	Moderate elongation defect
B0498.8	TES-1	0.5%	99.3%	Severe elongation defect
D2096.12	unknown	1.4%	98.3%	Severe elongation defect
T13F2.3	PIS-1	2.0%	98.8%	Severe elongation defect
F12F6.5	SRGP-1	0.6%	98.3%	Severe elongation defect
K01A6.1	MAGI-1	0.9%	98.4%	Severe elongation defect
Y62E10A.d	RLA-2	0.3%	95.9%	Severe elongation defect
Y67D8C.5	EEL-1	0.5%	95.2%	Severe elongation defect
C04E6.4	unknown	0.7%	90.0%	Moderate elongation defect
Y102A5A.1	CAND-1	0.1%	92.2%	Moderate elongation defect
K08B12.2	DMD-7	0.2%	88.0%	Moderate elongation defect
C50F4.11	MDF-1	1.5%	95.8%	Moderate elongation defect
R10D12.14	unknown	7.3%	95.3%	Moderate elongation defect
W08G11.4	PPTR-1	0.3%	99.8%	Moderate elongation defect
F25B3.1	EHBP-1	0.0%	85.0%	Moderate elongation defect
ZK218.4	unknown	0.0%	88.6%	Moderate elongation defect
C04F6.1	VIT-1	0.0%	100%	Severe/moderate elongation defect
K09F5.2	VIT-5	0.3%	100%	Moderate elongation defect
ZK1193.5	DVE-1	0.7%	85.0%	Moderate elongation defect
F02E8.3	APS-2	0.0%	99.6%	Moderate elongation defect
F26A10.2	unknown	0.2%	95.7%	Moderate elongation defect
F45E1.5	unknown	0.6%	99.9%	Moderate elongation defect
D2021.1	UTX-1	3.4%	99.9%	Severe elongation defect
T25B6.3	unknown	0.6%	96.1%	Moderate elongation defect
T20B5.1	APA-2	1.0%	99.8%	Severe elongation defect
F47A4.2	DPY-22	0.8%	98.3%	Moderate elongation defect
C44C10.8	HND-1	0.7%	98.7%	Moderate elongation defect
C44H4.2	SYM-5	11.0%	98.9%	Moderate elongation defect
C44H4.3	SYM-1	0.4%	97.8%	Moderate elongation defect
K10B3.10	SPC-1	5.7%	100%	Severe elongation defect
F22A3.1A	ETS-4	0.4%	95.6%	Moderate elongation defect
K08A8.1	MEK-1	0.2%	97.9%	Moderate elongation defect
ZK899.2	unknown	0.1%	94.7%	Moderate elongation defect
K09A9.3	ENT-2	0.7%	92.6%	Moderate elongation defect
C36E6.f	MLC-1	0.6%	96.3%	Moderate elongation defect
C12D12.1	unknown	0.4%	96.1%	Moderate elongation defect
F46H5.3	unknown	0.1%	87.0%	Moderate elongation defect
H13N06.2	unknown	0.2%	87.7%	Moderate elongation defect

Table S2. Candidate Genes Screened for an Ability to Affect MAGI-1::GFP Localization, Related to Figure 3

Reason screened	Genes screened
Proteins identified in *hmp-1(fe4)* enhancer screen with transmembrane domains	*ent-2, sym-1, sym-5,* C04E6.4, ZK218.4, ZK899.2
Orthologous to vertebrate Cadherin-23, which binds PDZ4 of vertebrate MAGI-1	*cdh-1*, *cdh-3*, *cdh-4*, *cdh-5*, *cdh-6, cdh-8*, *cdh-12*
Orthologous to JAM4, which binds vertebrate MAGI-1	*rig-1*, *unc-22*, *unc-89*
Orthologous to ESAM, which binds PDZ3 of vertebrate MAGI-1	*him-4*, *igcm-1*, *let-526, pxn-1*, *rig-5*, C01G8.9, F36A2.1, F56A12.1, T21B6.3, Y39D8B.1
Orthologous to Kir4.1, which binds vertebrate MAGI-1	*irk-1, irk-2, irk-3*
Orthologous to megalin, which binds vertebrate MAGI-1	*lrp-1, lrp-2,* T13C2.6
Orthologous to BAI1, which binds PDZ3 or PDZ4 of vertebrate MAGI-1	*adt-1, adt-2, gon-1, ppn-1,* C36B7.5, F09F9.4
Orthologous to Frizzled, which binds vertebrate MAGI-3	*cfz-2, lin-17, mig-1, mom-5*
C. elegans cell adhesion receptors	*cdh-7, cdh-9, cdh-10, cdh-11, clc-1, clc-2, clc-3, clc-4, coh-1 crb-1, csp-2, dgn-1, eat-20, glit-1, hmr-1, ina-1, itx-1, lad-2, lat-1, lat-2, let-805, mua-3, ncam-1, nlr-1, nrx-1, nsy-4, pat-2, pat-3, rig-3, rig-4, rig-6, sax-3, sax-7, slo-1, stg-1, stg-2, syd-1, syd-2, syg-1, syg-2, vab-9, wrk-1,* C24H10.1, C48E7.6, C54G4.4, D2096.11, K10D6.2, M116.5, R04F11.1, T17A3.10, R04F11.1

Supplemental Experimental Procedures

Strains and Alleles

Standard methods were used for maintaining and handling worms [1]. Experiments (unless otherwise noted) were conducted at 20ºC and the *C. elegans* Bristol strain N2 was used as wild-type. The following mutations were used: Linkage group II: *hmp-2(qm39)* [2], *vab-9(ju6)* [3]; Linkage group IV: *magi-1(zh66)* [4], *sax-7(eq1)* [5]; Linkage group V: *hmp-1(fe4)* [6]. The following transgenic lines were used: *dlg-1::gfp* [7], *hmp-2::yfp* [4], *jcIs17* [8], *magi-1::gfp* [4], *magi-1::mRFP* [9], and *vab-10ABD::gfp* [10]. To generate worms carrying both *hmp-2(qm39)* and *magi-1(zh66)*, *hmp-2(qm39)* homozygous males were mated with *magi-1(zh66)* homozygous hermaphrodites. F1 progeny were singled and genotyped for *magi-1(zh66)* to identify heterozygous *magi-1(zh66)* hermaphrodites. F2 progeny were singled from heterozygous F1 worms and allowed to lay progeny. Adult F2 worms were genotyped for the *magi-1(zh66)* allele and lethality counts were performed on the progeny to determine the *hmp-2* genotype. The *magi-1(zh66)*/*magi-1(zh66)*; *jcIs17* strain was generated using a similar method. The *(zh66)* allele was tracked via PCR and *jcIs17* was identified using the *rol* marker that is part of the insertion sequence.

RNAi

Feeding RNAi was performed as previously described [11]. Briefly, bacteria carrying a plasmid encoding a piece of *C. elegans* genomic DNA was induced using IPTG and fed to L4 stage worms for 48 hours. Phenotypes were assessed in the next generation. Injection dsRNA-mediated interference was performed as previously described [12]. Single-stranded RNA was transcribed and purified using the Ambion MegaScript T3 and T7 kits according to the manufacturer's protocol. Individual RNAs were injected at 2 mg/ml. Partial cDNA clones used as templates for the RNA transcription were as follows: yk1448f6 (*magi-1*), yk662b10 (*hmr-1*), yk25e5 (*dlg-1*), yk484c4 (*crb-1*), yk524b7 (*let-413*), yk766b4 (*sax-7*), yk1725g10 (*afd-1*), yk1182e9 (*rig-1*), yk1008b11 (*igcm-1*), yk475h2 (*lad-2*), yk1291f8 (*rig-4*), yk1115b7 (*csp-2*), and yk1130b8 (*lin-17*). All clones were a kind gift from Yuji Kohara (National Institute of Genetics, Japan).

Plasmids

Yeast two-hybrid bait constructs encoding *sax-7* (pLC209) and *sax-7ΔCT* (pLC228) and the yeast two-hybrid prey constructs encoding PDZ1-2 (pLC244) and PDZ1-5 of *magi-1* (pLC232) were a kind gift of Lihsia Chen (University of Minnesota). Yeast two-hybrid bait constructs encoding the RA1-2 domains (pIC198) and the DIL-PDZ domains (pIC249) of *afd-1* were a kind gift of Ian Chin-Sang (Queen's University, Ontario, Canada). The yeast two-hybrid prey construct containing PDZ3 was generated by amplifying the corresponding region of *magi-1* from a cDNA library made using wild-type worms. The primers used had restriction sites on their ends and the resulting PCR product and pGADT7 were digested using BamHI and EcoRI. The digested products were gel purified, ligated together overnight, and transformed the following day into DH5α *E. coli*. Transformants were screened via PCR amplification of PDZ3 and positive clones were sequenced to confirm their identity. The yeast two-hybrid construct containing PDZ4-5 was generated by round-the-world drop out PCR of pLC232 using primers that flanked PDZ1-3. The resulting product was DpnI digested, incubated with T4PNK for 30 minutes, ligated together overnight, and transformed the following day into DH5a *E. coli*.

Transformants were screened by PCR to detect PDZ4-5 and positive clones were sequenced to confirm the deletion.

Directed Yeast Two-Hybrid Tests

Yeast bait and prey constructs were transformed separately and together into Y2Hgold yeast from Clontech. Positive transformants were selected using SD/-leu, SD/-trp, and SD/-leu/-trp plates. Single transformants were patched onto SD/-leu/Xαgal or SD/-trp/Xαgal plates to test for autoactivation. None of the baits or prey displayed any significant autoactivation (data not shown). Double transformants were patched onto SD/-leu/-trp/Xαgal/AurA plates to test for interaction. Positively interacting clones were capable of growth in the presence of AurA and turned blue due to the presence of Xαgal.

Microscopy

4D Nomarski microscopy was performed as previously described [13]. Embryos were filmed on a Nikon Eclipse E600 or Optiphot-2 upright microscope equipped with DIC optics. ImageJ software with custom plugins was used to compress 3D time-lapse data into 4D QuickTime movies for analysis (J. Hardin; available at http://worms.zoology.wisc.edu/research/4d/4d.html). Spinning disc confocal microscopy on live GFP embryos was performed with a Yokogawa CSU10 scanhead attached to a Nikon Eclipse E600 microscope. Data were collected with a Hamamatsu ORCA-ER CCD camera using Perkin Elmer Ultraview software. Images were analyzed using ImageJ and Volocity (Perkin Elmer) and figures were prepared using Illustrator (Adobe).

Measuring Expression of Junctional Reporters

The expanse of AJM-1 expression in *sax-7(eq1)* and *magi-1(zh66)* embryos compared to wild-type embryos was measured by reslicing through junctions stained with MH27. Using ImageJ software, three depths along the junction were measured and then averaged together to determine the junction depth for an embryo. For each genotype, junction depths were averaged, the standard deviation was calculated, and the significance of differences in junction depth measurements among the genotypes was calculated using a two-tailed Student's t-test. The expression domain of HMP-1::GFP in *jcIs17* and *magi-1(zh66); jcIs17* embryos was measured by imaging embryos at ~1.5 fold stage of development. The 8^{th} seam cell from the anterior was identified and the width of expression was measured along all sides of the junction using ImageJ software. The values were averaged together to determine the average junction width for an embryo. For both genotypes, junction widths were averaged, the standard deviation was calculated, and the significance of differences in junction width between the genotypes was calculated using a two-tailed Student's t-test.

Staining

Antibody staining was performed using a freeze-cracking method as described previously [14]. Primary antibodies in PBST+dry milk were applied overnight at 4ºC to embryos. Secondary antibodies in PBST+dry milk were applied for ~3 hours at room temperature. The following antibodies were used: 1:50-1:1000 Rb-α-MAGI-1 (kind gift of Chris Rongo), 1:10 Rb-α-AFD-1, and 1:200-1:400 M-α-AJM-1 (MH27). Secondary antibodies include: 1:50 αRb-FITC, 1:50

αRb-Texas Red, 1:50 αM-FITC 1:50 αM-Texas Red. For phalloidin staining, embryos were fixed and permeabilized as has been previously described [15]. Stained embryos were visualized using spinning disc confocal microscopy as described above.

FRAP

Gravid adults were bisected in M9 solution and embryos collected. Embryos were transferred by mouth pipette to a 5% agar pad on a glass slide, submerged in M9 and sealed with a glass cover slip for filming. Embryos were aged until they were approximately comma stage and embryos carrying fluorescently tagged proteins were identified. A region of interest for photobleaching was identified, as was a control region using Fluoview ASW-v1.7 software. Embryos were photobleached and then continuously filmed to assay recovery using an Olympus Fluoview 1000 confocal microscope. Data was analyzed using a custom set of FRAP plugins developed for ImageJ (J. Hardin; available at http://worms.zoology.wisc.edu/research/4d/4d.html). Significance was calculated using a 2-tailed Student's T-test.

Supplemental References

1. Brenner, S. (1974). The genetics of Caenorhabditis elegans. Genetics *77*, 71-94.
2. Lockwood, C., Zaidel-Bar, R., and Hardin, J. (2008). The C. elegans zonula occludens ortholog cooperates with the cadherin complex to recruit actin during morphogenesis. Curr Biol *18*, 1333-1337.
3. Simske, J.S., Koppen, M., Sims, P., Hodgkin, J., Yonkof, A., and Hardin, J. (2003). The cell junction protein VAB-9 regulates adhesion and epidermal morphology in C. elegans. Nat Cell Biol *5*, 619-625.
4. Stetak, A., Horndli, F., Maricq, A.V., van den Heuvel, S., and Hajnal, A. (2009). Neuron-specific regulation of associative learning and memory by MAGI-1 in C. elegans. PLoS One *4*, e6019.
5. Wang, X., Kweon, J., Larson, S., and Chen, L. (2005). A role for the C. elegans L1CAM homologue lad-1/sax-7 in maintaining tissue attachment. Dev Biol *284*, 273-291.
6. Pettitt, J., Cox, E.A., Broadbent, I.D., Flett, A., and Hardin, J. (2003). The Caenorhabditis elegans p120 catenin homologue, JAC-1, modulates cadherin-catenin function during epidermal morphogenesis. J Cell Biol *162*, 15-22.
7. Koppen, M., Simske, J.S., Sims, P.A., Firestein, B.L., Hall, D.H., Radice, A.D., Rongo, C., and Hardin, J.D. (2001). Cooperative regulation of AJM-1 controls junctional integrity in Caenorhabditis elegans epithelia. Nat Cell Biol *3*, 983-991.
8. Zaidel-Bar, R., Joyce, M.J., Lynch, A.M., Witte, K., Audhya, A., and Hardin, J. (2010). The F-BAR domain of SRGP-1 facilitates cell-cell adhesion during C. elegans morphogenesis. J Cell Biol *191*, 761-769.
9. Emtage, L., Chang, H., Tiver, R., and Rongo, C. (2009). MAGI-1 modulates AMPA receptor synaptic localization and behavioral plasticity in response to prior experience. PLoS One *4*, e4613.
10. Gally, C., Wissler, F., Zahreddine, H., Quintin, S., Landmann, F., and Labouesse, M. (2009). Myosin II regulation during C. elegans embryonic elongation: LET-502/ROCK, MRCK-1 and PAK-1, three kinases with different roles. Development *136*, 3109-3119.
11. Kamath, R.S., and Ahringer, J. (2003). Genome-wide RNAi screening in Caenorhabditis elegans. Methods *30*, 313-321.
12. Walston, T., Tuskey, C., Edgar, L., Hawkins, N., Ellis, G., Bowerman, B., Wood, W., and Hardin, J. (2004). Multiple Wnt signaling pathways converge to orient the mitotic spindle in early C. elegans embryos. Dev Cell *7*, 831-841.
13. Raich, W.B., Agbunag, C., and Hardin, J. (1999). Rapid epithelial-sheet sealing in the Caenorhabditis elegans embryo requires cadherin-dependent filopodial priming. Curr Biol *9*, 1139-1146.
14. Williams-Masson, E.M., Malik, A.N., and Hardin, J. (1997). An actin-mediated two-step mechanism is required for ventral enclosure of the C. elegans hypodermis. Development *124*, 2889-2901.
15. Costa, M., Raich, W., Agbunag, C., Leung, B., Hardin, J., and Priess, J.R. (1998). A putative catenin-cadherin system mediates morphogenesis of the Caenorhabditis elegans embryo. J Cell Biol *141*, 297-308.